Anle138b interaction in α-synuclein aggregates by dynamic nuclear polarization NMR

Rıza Dervişoğlu,[a, b, #] Leif Antonschmidt,[a, #] Evgeny Nimerovsky,[a] Vrinda Sant,[a] Myeongkyu Kim,[a] Sergey Ryazanov,[a, c] Andrei Leonov,[a, c] Juan Carlos Fuentes-Monteverde,[a] Melanie Wegstroth,[a] Karin Giller,[a] Guinevere Mathies,[d] Armin Giese,[c] Stefan Becker,[a] Christian Griesinger [a, e] and Loren B. Andreas [*a]

Sensitivity comparison

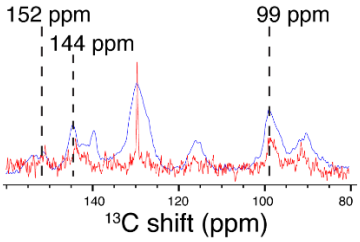

Figure S1. ^{13}C CP spectra at 300 K without DNP (red, 6144 scans) and after addition of biradical and cryoprotectant with microwaves on at 100 K (blue, 1024 scans) showing the aromatic region. The sample is the ^{15}N labelled αS fibril grown in the presence of ^{13}C labelled anle138b. Vertical dashed lines indicate resonances assigned to anle138b, as detailed in Fig. 3. DNP enhanced ssNMR spectra were recorded with MAS of 12.5 kHz at a temperature of 100 K while the 850 MHz spectra were recorded with 17.5 kHz MAS (scaled up with field) at a temperature of 300 K, no TEMTriPol. Note that the DNP spectrum was acquired for substantially more time than the microwaves ON/OFF comparison of Figure 2A.

Considering that sensitivity increases with $B_0^{3/2}$, and T^{-1}, 600 MHz at 100 K has a 1.8-fold theoretical sensitivity improvement over 850 MHz at 300 K. This does not consider the DNP effect, changes in T_1, linewidths, and probe performance.[1] Including the DNP enhancement of ~8-fold as observed in Figure 2A, then ~14 fold improvement (1.8 x 7) is expected for the 600 MHz at 100 K with DNP over 850 MHz at 300 K. The approximately 4 to 10-fold observed improvement (Table S1), rather than the full 14, can be explained by the longer recycle-delay at DNP conditions, broader linewidths at low temperature, dilution of the sample after addition of biradical and cryoprotectant, and probe performance. The sensitivity was assessed for a protein aromatic signal at about 130 ppm as well as for an anle138b peaks. The experimental conditions were 4 s recycle-delay (RD) on the 600 MHz DNP system (T_1 = 3 s) and an RD of 2 s on the 850 MHz spectrometer (T_1= 0.5 s). Note that the RD at the 850 MHz spectrometer was chosen to avoid excessive sample heating, and is substantially longer than the optimum based on T_1. Using the αS fibril aromatic ^{13}C signal at 129 ppm (signal: 124-133 ppm, noise: 102-111 ppm) we observe a 4.1-fold sensitivity improvement. Using the anle138b peak at 99 ppm (signal: 124-133 ppm, noise: 102-111 ppm) we observe 10.3-fold gain in sensitivity. Sensitivity was calculated according to:

$$Sensitivity = \frac{S/N(600) \Big/ \sqrt{NS(600) \times RD(600)}}{S/N(850) \Big/ \sqrt{NS(850) \times RD(850)}}$$

where S/N is the signal to noise ratio as read from spectra by Bruker Topspin 3.5 software using the SINO command, NS is the number of scans and RD is the recycle

delay. Note that the processing of the data was optimized for the sharp aromatic signal at 130 ppm and may overestimate the gain for the broader signals from anle138b. On the other hand, the enhancement factor was relatively low for this particular sample, underestimating the possible improvement.

Table S1: Experimental observables used for the calculation of the sensitivity gain with the DNP system.

Parameter	600 MHz DNP exp.* (15.08.2019 exp. 16)	850 MHz room temp. exp.# (23.05.2019 exp. 33)
S/N (SINO) for the protein aromatics / (Signal 124-133 ppm; Noise 102-111ppm)	31.38	13.17
S/N (SINO) for the anle138b peak / (Signal 94-100 ppm; Noise 103-109)	19.84	3.35
Number of Scans (NS)	1024	6144
Recycle delay (RD) / s	4	2
Sensitivity (Signal 124-133 ppm; Noise 102-111ppm) / $s^{-0.5}$	0.49	0.12
Sensitivity (Signal 94-100 ppm; Noise 102-111ppm) / $s^{-0.5}$	0.31	0.03

* 600 MHz magnetic field, 12.5 kHz spinning frequency, 100 K, ^{1}H-^{13}C Cross Polarization experiments with 0.9 ms contact time, 96-107 kHz ^{1}H and 112 kHz ^{13}C pulse power.
# 850 MHz magnetic field, 17.5 kHz spinning frequency, 300 K, ^{1}H-^{13}C Cross Polarization experiments with 3 ms contact time, 69-76 kHz ^{1}H and 60 kHz ^{13}C pulse power.

EPR analysis of Max Planck Institute for Multidisciplinary Sciences (MPINAT) synthesized TEMTriPol-1

X-band EPR spectroscopy of TEMTriPol-1 (Figure 2) synthesized at the facility for Synthetic Chemistry at Max Planck Institute for Multidisciplinary Sciences, Göttingen (MPINAT) was performed at room temperature and under cryogenic conditions (120 K). The spectra are compared to those of TEMTriPol-1 synthesized in the laboratory of Dr. Yangping Liu at Tianjin Medical University,[2-3] see the Figures S2 and S3 below.

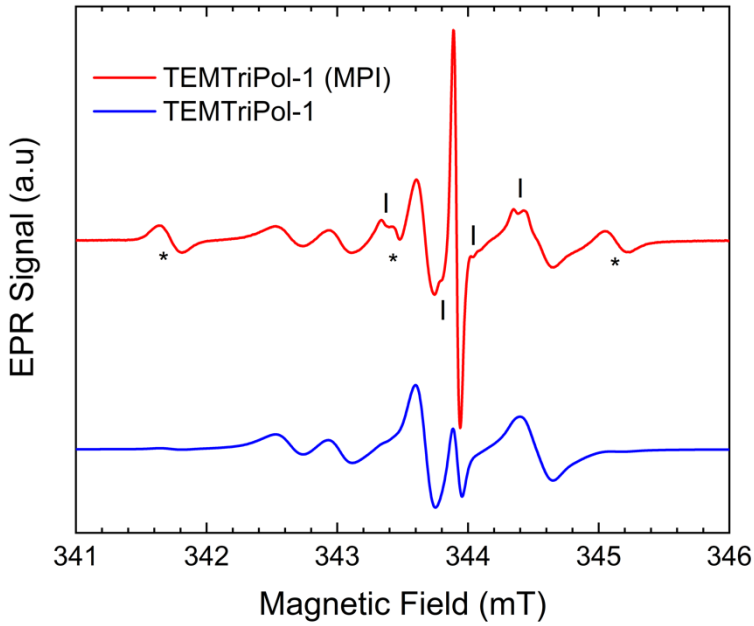

Figure S2: Continuous-wave EPR spectra of TEMTriPol-1 in deionized water at room temperature. Microwave frequency: 9.6439 GHz, modulation amplitude: 0.04 mT, microwave power: 10 mW.

The spectrum of TEMTriPol-1 (MPI) in Figure S2 (red) contains the features associated with TEMTriPol-1 (blue), most prominently the double signal centered at 342.8 mT. However, the TEMTriPol-1 (MPI) spectrum also shows other features, which do not arise from TEMTriPol-1. These are: the three signals indicated by *, a strong, narrow signal centered at 343.9 mT, and four weak signals marked with vertical lines. These signals arise, respectively, from 4-amino-TEMPO (or a related mono-nitroxide radical with A_{iso} = 48 MHz for the hyperfine interaction with ^{14}N) and mono-trityl (presumably Finland trityl), of which the central line as well as some of the satellite lines are visible. Thus, the TEMTriPol-1 (MPI) preparation contains, besides the biradical TEMTriPol-1, a significant amount of mono-radical. We estimate that these mono-radicals make up about 50 % of the total radical concentration.

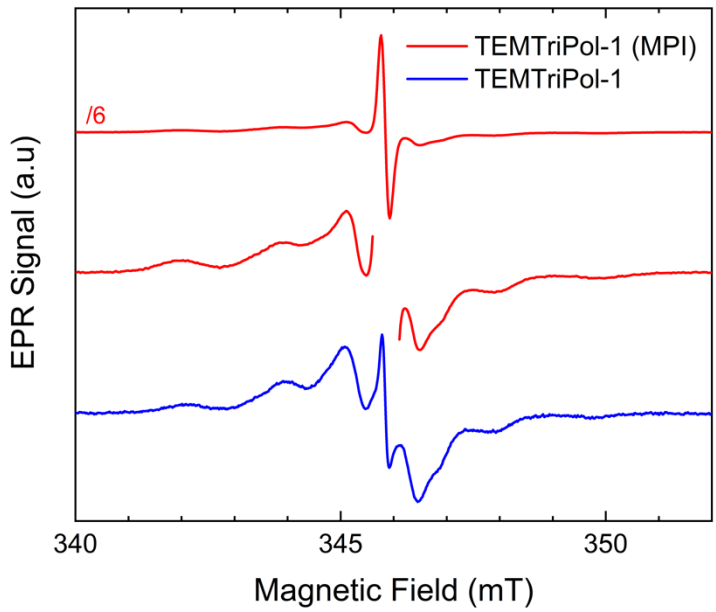

Figure S3: Continuous-wave EPR spectra of TEMTriPol-1 in DNP juice (glycerol-d_8/D_2O/H_2O 60:30:10 vol%) at 120 K. Microwave frequency: 9.7018 GHz, modulation amplitude: 0.1 mT, microwave power: 0.5 mW.

To determine the concentration of TEMTriPol-1 (MPI) in the samples of α-synuclein with anle138b prepared for DNP MAS NMR, a diluted aliquot of the supernatant was investigated by EPR spectroscopy at 120 K (Figure S3, red curves). Comparison of this spectrum to the spectrum of TEMTriPol-1 (blue) indicates again that a fraction of mono-nitroxide and mono-trityl is present in the TEMTriPol-1 (MPI) preparation. This is obvious from the strong narrow line of mono-trityl at 345.8 mT and the extra intensities observed at the high- and low-field edges of the TEMTriPol-1 (MPI) spectrum, at 342 and 350 mT, which arise from the mono-nitroxide fraction. Double integration of the TEMTriPol-1 (MPI) spectrum and comparison to a reference of 4-oxo-TEMPO indicates a total radical concentration in the α–synuclein/anle138b samples of 16 mM. Assuming these are all biradicals (which is clearly not the case), this places an upper limit of 8 mM on the biradical concentration in the DNP samples investigated in this work.

TEMTriPol-1 radical synthesis and stability

The TEMTriPol-1 was synthesized in 2018 by the laboratory of Dr. V. N. Belov (the facility for Synthetic Chemistry at Max Planck Institute for Multidisciplinary Sciences, Göttingen (abbreviated here as MPI)) following the existing literature by Liu et al.[2] Prepared TEMTriPol-1 (MPI) was pure by its HPLC chromatogram. Its mass spectrum: ESI(+)-MS $[M+H]^+$ 1211.4; and ESI(-)-MS $[M-H]^-$ 1209.4; and UV (CH_3CN/H_2O): λ_{max} 268.9, 336.1, 466.7 nm were in agreement with values reported.[2] The HPLC chromatogram and UV/Vis spectrum are shown in Figure S4.

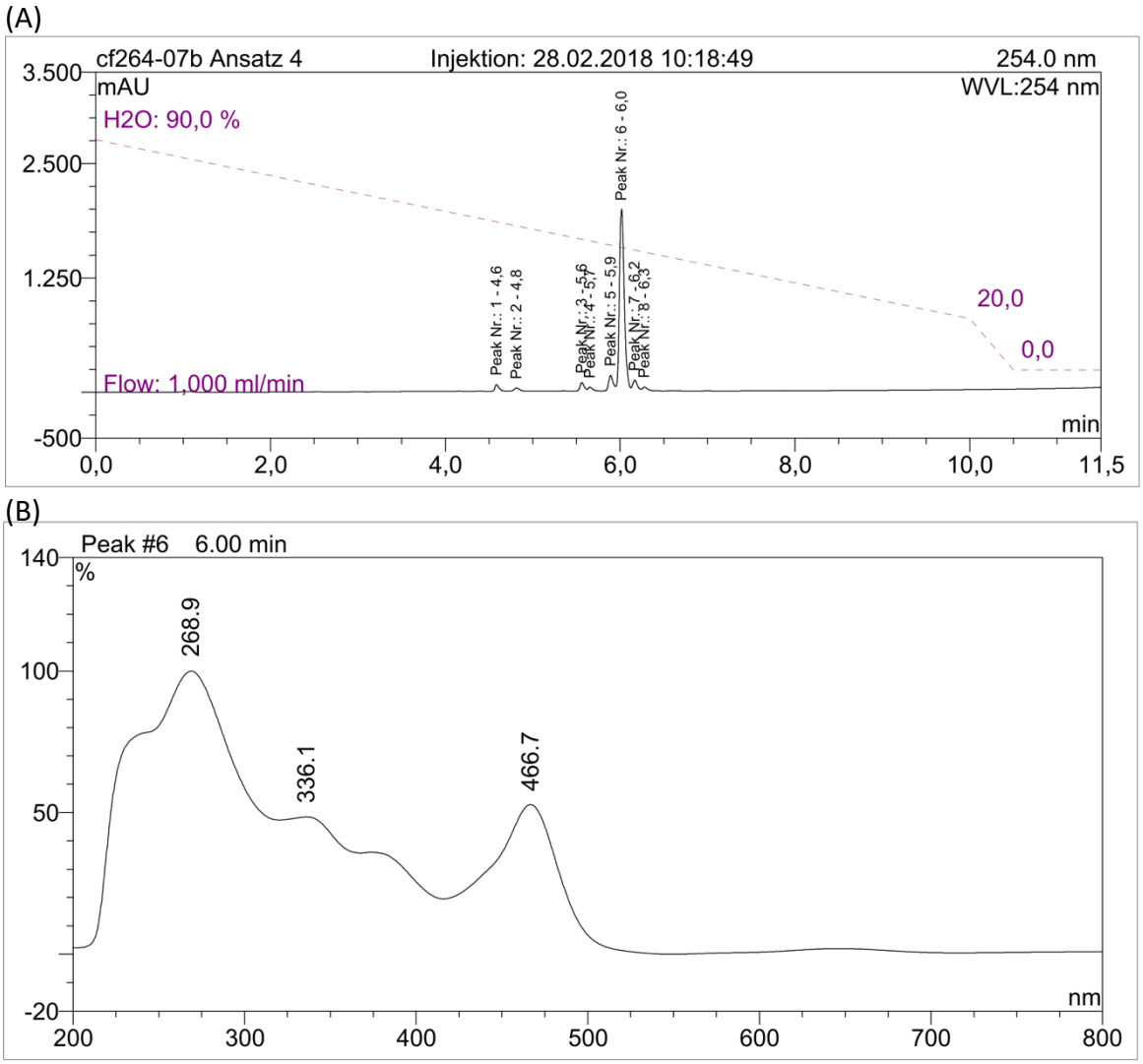

Figure S4 UV/Vis-HPLC detection of TEMTriPol-1 (MPI). (A) HPLC chromatogram of the TEMTriPol-1 sample. (B) UV/Vis showing the peak with retention time of 6.00 min (λ_{max} = 268.9, 336.1, 466.7 nm). Chromatographic conditions: Column Kinetex C18 (100 Å 7.5 cm x 4.6 mm, 2.6 µm) (Phenomenex); 10-min gradient from 10 to 80 vol% of CH_3CN/H_2O, then 0.5 min gradient from 80 vol% of CH_3CN/H_2O to 100 vol% CH_3CN, finally 1 min of isocratic elution (100 vol% CH_3CN); flow rate, 1 mL min^{-1}. The chromatography gradient, based on the water percentage, is indicated by a dashed purple line in (A). Sample was synthesized at MPINAT in 2018.

Following our EPR results we have analyzed the TEMTriPol-1 radical for chemical stability/integrity comparing two time points 2018, right after the synthesis, and 2021, after 3 years at -20 °C in solid form under nitrogen atmosphere. We do not observe a major structural chemical decomposition and the sample is pure, namely the chromatographic behavior stays the same over time without generation of multiplets, keeping the retention time (Δt_R = 0.1 min) and the UV spectral features. The HPLC chromatogram and the UV/Vis spectrum of the major peak are seen in Figure S5. These findings lead to the conclusion that the bi-radical TEMTriPol-1 from MPINAT, was in 2018 and still (2021) is a partial mono-radical. We believe this happens in a manner of quenching either the nitroxide or trityl part of the bi-radical in the absence of stabilizers for the pure compound. Such a need for stabilization is reported for some

other radicals not used in the present work, such as galvinoxyl, where phenolic-antioxidants, including some precursors for the radical itself, act as a stabilizer but pure-radical-crystals go through a quenching process.[4-5] However, even after the formation of the TEMTripol-1 derived mono-radical the existing bi-radical and mono-radical mixture is capable of performing well for DNP of membrane protein samples as shown in the main paper (Figure 2).

(A)

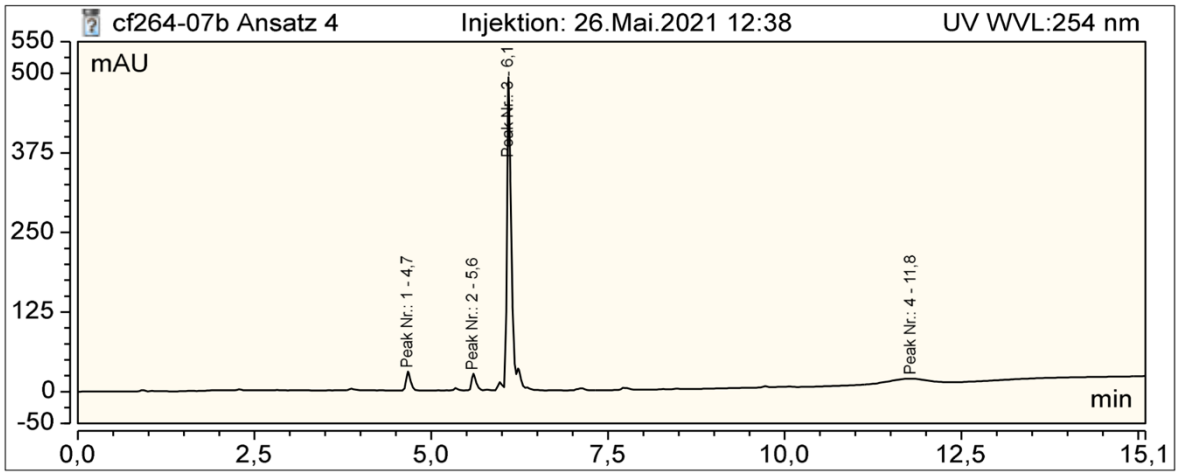

(B)

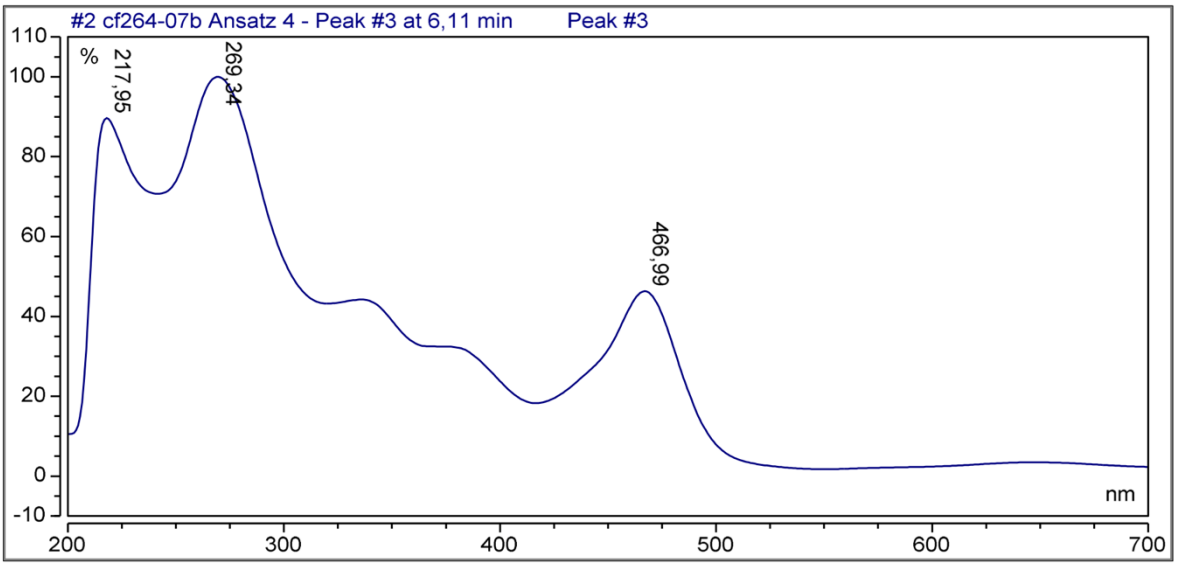

Figure S5: UV/Vis-HPLC of TEMTriPol-1 after 3-year storage. (A) HPLC chromatogram of a stock solution eluted with CH_3CN/ H_2O (10-80 vol%) containing TEMTriPol-1; (B) UV/Vis (λ_{max} = 269.3, 337.5, 467.0 nm) showing the peak with retention time of 6.10 min. The sample, a solid green crystalline powder, was synthesized at MPINAT in 2018, and analyzed in 2021 after storage at -20 °C temperature under N_2 atmosphere. Chromatographic conditions were the same as in figure S4.

REDOR data for a known bond length, with fit background signal

The performance of the Rotational Echo Double Resonance (REDOR) measurement was assessed for a known one-bond signal observed at the protein carbonyl (Figure 6A-B). This verifies good performance of the sequence even for long mixing times of beyond 20 ms. Minimal decay is observed for the long mixing times, as expected based on simulated REDOR curves. However, the REDOR signal reaches a relatively low value of about 0.7, suggesting that part of the signal does not dephase. The REDOR data fits a 1.3 Å distance (Figure 6B) with 70% population dephased, matching the one-bond nitrogen-carbonyl interaction. The 30% population that does not show dephasing is interpreted to be due to the lipid carbonyls without nitrogens nearby. Fits for 1 or two couplings are shown for the 152-ppm peak in Figure S6C, and indicate a distance below about 5 Å. The signal-to-noise ratio of this peak is relatively low, motivating analysis of the C_5 peak, and the C_4 peak with FS-REDOR (see Figures S7 and S16).

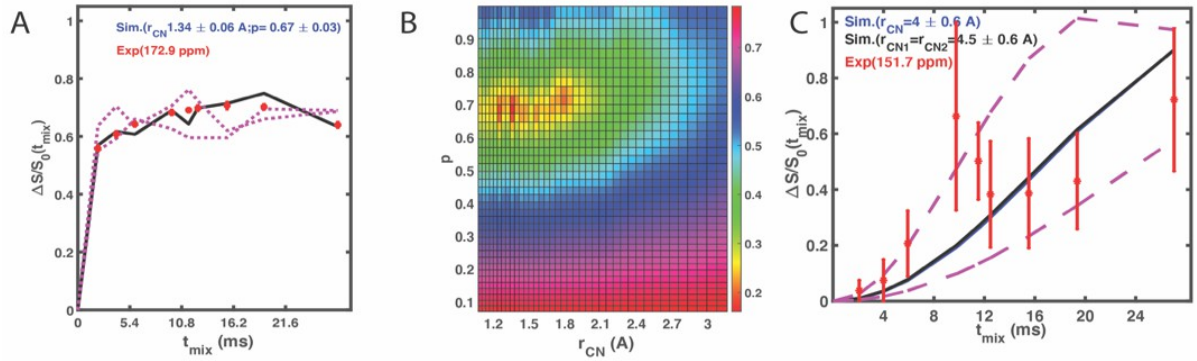

Figure S6 (A) Experimental (red stars) and simulated (lines) ^{13}C-^{15}N REDOR ΔS/S0 curves for a 1-bond N-C distance in αS. The backbone carbonyl (^{13}C, 173 ppm) signal at natural abundance is modulated by the labelled backbone ^{15}N. (B) RMSD between simulated and experimental data, for different distances and populations, with the best fit at 1.3 Å and 70 % population. The population of less than one takes into account that there is overlapping lipid signal that is not near a ^{15}N spin. The determined distance of 1.34 Å reproduces very well the published CN distance of 1.32 Å. (C) Distance fit for the 152-ppm peak of ^{13}C labelled anle138b reproducing the result of ~4.4 Å distance between C_5 of anle138b and ^{15}N backbone of αS with a larger error margin compared to the 144-ppm peak that is reported in the SI and in Figure S7.

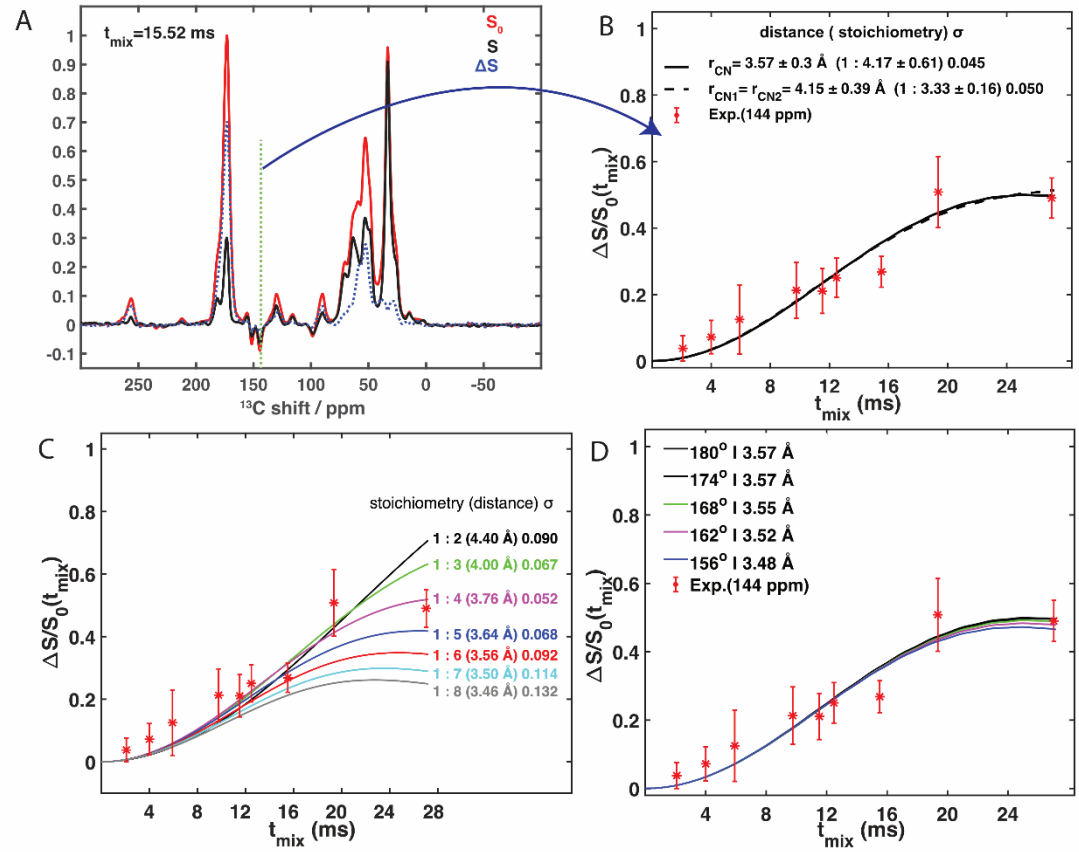

Figure S7 Distance fitting with ^{15}N-^{13}C REDOR using DNP showing the impact of multiple ^{15}N spins which each cause REDOR dephasing. Example spectra are shown in (A) for 15.52 ms of REDOR. In (B), the 144-ppm peak (C_5) intensity of anle138b is analyzed as a function of mixing time, as $\Delta S/S_0$ (red stars). The fit by numerical REDOR simulations (solid), results in a distance between C_5 of drug and ^{15}N of protein of 3.6 ± 0.3 Å, when fit to a single coupling. The molar ratio of anle138b:αS in the complex was simultaneously fit (together with the known starting molar ratio of 1:2) to about 1:4. Interaction to two equidistant nitrogens is also simulated, indicated by dashed lines. The anle138b:αS ratio then fit to ~1:3.3, and the fit distance increased to 4.15. Additional couplings further increase the fit distance (see Figure S16). (C) Simulations of various anle138b to αS monomer stoichiometries with corresponding distances in brackets and standard deviation (σ) together with experimental data points. The binding stoichiometry strongly impacts the shape of the fit curves. (D) Simulations with various small pulse angle differences from 180° (lines) are superimposed on the experimental points. The fit deviates less than 0.1 Å even at 24° deviation from 180°. Spectra were recorded at 14.1 T under DNPMAS conditions. Error bars are estimated based on spectral signal/noise and are shown at 1 root-mean-squared.

REDOR Simulations

The simulated REDOR curves were obtained with in-house MATLAB code, the details of which can be found in previous work.[6-7] The best distances as well as the errors were obtained by minimization of the root-mean-square deviation (RMSD). The distance errors were calculated by adding the noise level into measured S and S_0 values.

To more quantitatively characterize the distances between pyrazole carbons and the protein backbone, we recorded REDOR spectra.[8-11] REDOR spectra of ^{13}C labelled anle138b dephased by ^{15}N-labelled αS fibril are shown in Figure S7. The anle138b

signals at 15.52 ms (one out of nine rotor synchronized time periods observed) are negative due to the $^{13}C,^{13}C$ ^{1}J-coupling between $C_{3/5}$ and C_4 with $\cos(\pi*65.3Hz*15.52\ ms) \approx -1$. The relatively large dephasing value of 0.26 at 15.52 ms, indicates that a substantial fraction of the anle138b is in contact with the protein. For quantitative fitting we have to consider the fraction of bound anle138b, and also unbound anle138b molecules, the latter of which do not experience signal dephasing. The spectra are sensitive to not only the distance but also the number of nitrogens in close proximity to the carbons. In Figure S7B, assuming a single carbon-nitrogen dipolar interaction a distance of 3.6 ±0.3 Å is fit to the more intense peak at 144 ppm. If two equidistant nitrogen spins are considered to dephase the carbon, the distance is increased above 4 Å.

An unbound fraction is expected if one considers a low binding stoichiometry. In fact, a 50 % bound fraction implies a stoichiometry of 1:4 (anle138b:αS monomer), suggesting there may be sufficient anle138b for saturation of more than one binding site at these relatively high concentrations. The best fit of REDOR simulations results in a 3.6 ± 0.3 Å distance to a single nitrogen with stoichiometry of 1:4.17, in good agreement with the size of the molecule and binding along the fibril axis (Figure 3B). Figure S7C and S7D explore the impact of stoichiometry and pulse imperfections on REDOR fitting. These data emphasize the difficulty of fitting REDOR data when there are a large number of dephasing spins. Nevertheless, the bound population, which depends on the stoichiometry of the bound complex, was relatively consistent.

Potential Impact of DNP sample conditions

'Fingerprint' spectra (Figure S8) of fibrils demonstrate minimal chemical shift perturbations upon addition of glycerol and TEMTriPol-1 for DNP. This indicates that the fibril remains after addition of glycerol. Similar fingerprint spectra for oligomer are shown in Figure S9-S10.

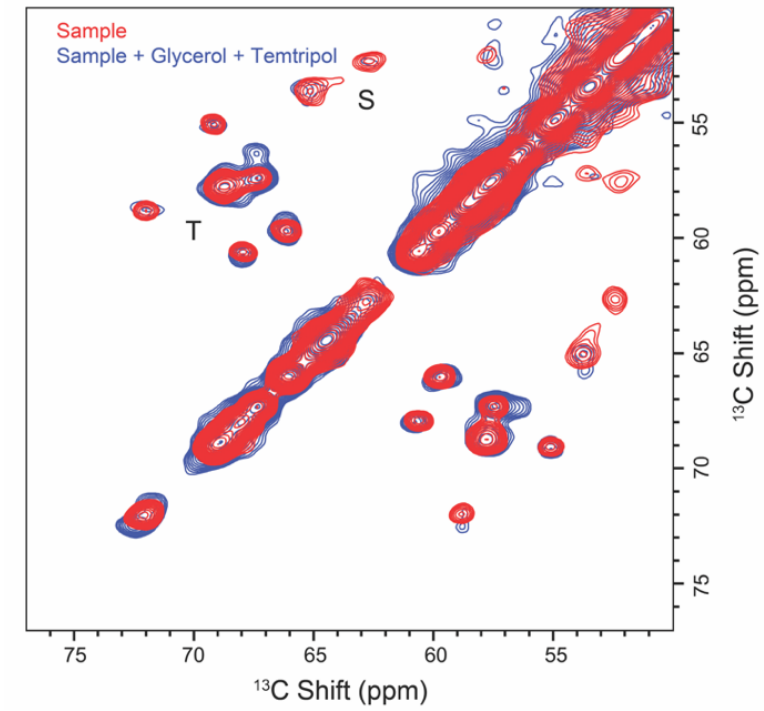

Figure S8. 2D RFDR ^{13}C-^{13}C with 1.3 ms mixing before (red) and after (blue) addition of components needed for DNP. αS fibrils grown in the presence of anle138b (red - sample) are compared with the same fibrils containing anle138b, after addition of glycerol and TEMTriPol-1 for DNP measurements (blue). Both experiments were performed at 300 K at 850 MHz NMR magnet with 17 kHz MAS.

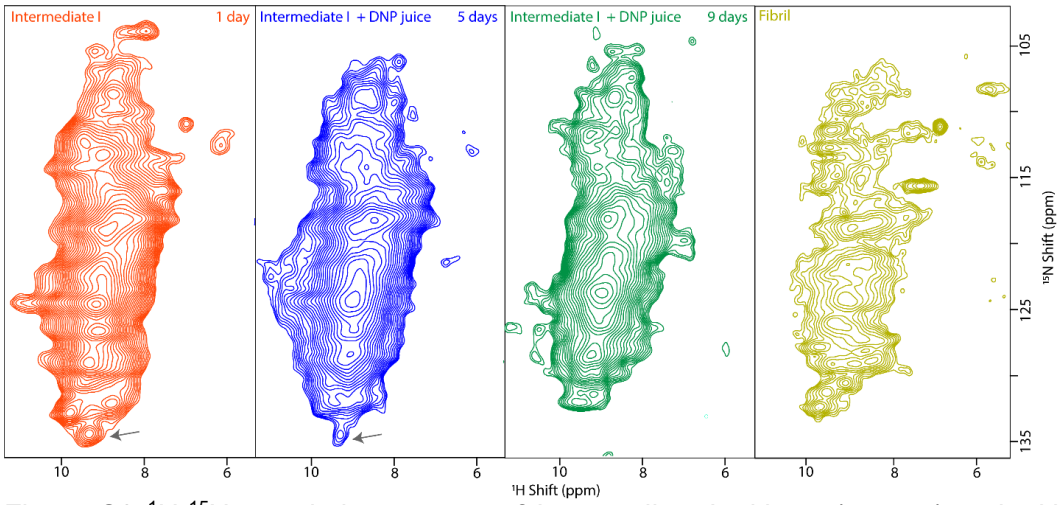

Figure S9 ^{1}H-^{15}N correlation spectra of Intermediate-I without (orange) and with (blue and green) the DNP juice. The spectrum of the fibril is shown in yellow. The ^{15}N peak at 135 ppm (grey arrow) is unique to Intermediate-I as compared to the fibril (yellow spectrum). Intermediate-I is a transient sample and we observe that it generally remains stable for periods of 5 – 20 days. In the case shown, we observe that after addition of DNP juice, the characteristic ^{15}N peak at 135 ppm persists (5-day sample), indicating the stability of Intermediate-I in a glycerol matrix. However, over the course of time (9 days) at 290 K the spectrum evolves, and the characteristic peak is no longer observed. This re-iterates the need for freezing the intermediate samples as performed for the DNP MAS NMR experiments that are frozen in liquid nitrogen immediately after addition of DNP juice, and remain stable in a glycerol matrix. The sample at 9 days has not yet converted completely to fibril.

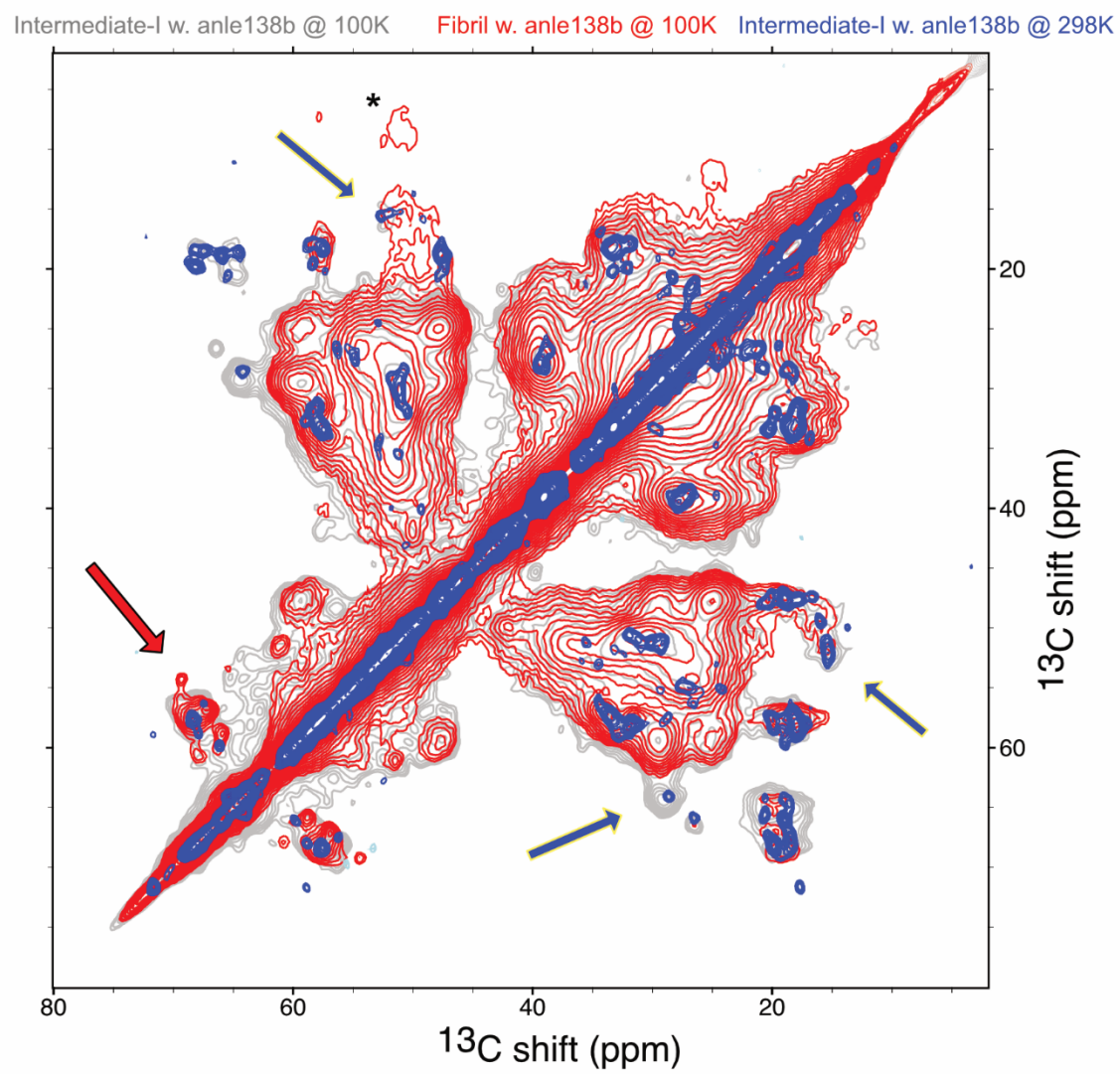

Figure S10. ^{13}C-^{13}C correlation spectra of the Intermediate-I (grey, same sample as in Figure 4C) at 100 K with DNP juice, fibril (red) at 100 K with DNP juice and Intermediate-I (blue) at 290 K on an 850 MHz magnet without the DNP juice. The similarities of the blue and the grey spectra indicated with blue arrows show the integrity of the Intermediate samples containing glycerol as in the DNP juice for these measurements. The red arrows indicate the unique shifts belonging to the αS fibrils. The "*" denotes the second spinning side band of the carbonyl.

Characterization of potential background signals near anle138b peaks

Sideband intensities or protein side-chain resonance are found near the anle138b peaks. Figure S11 compares samples with and without anle138b which demonstrate minimal background, in particular for the peak at 144 ppm.

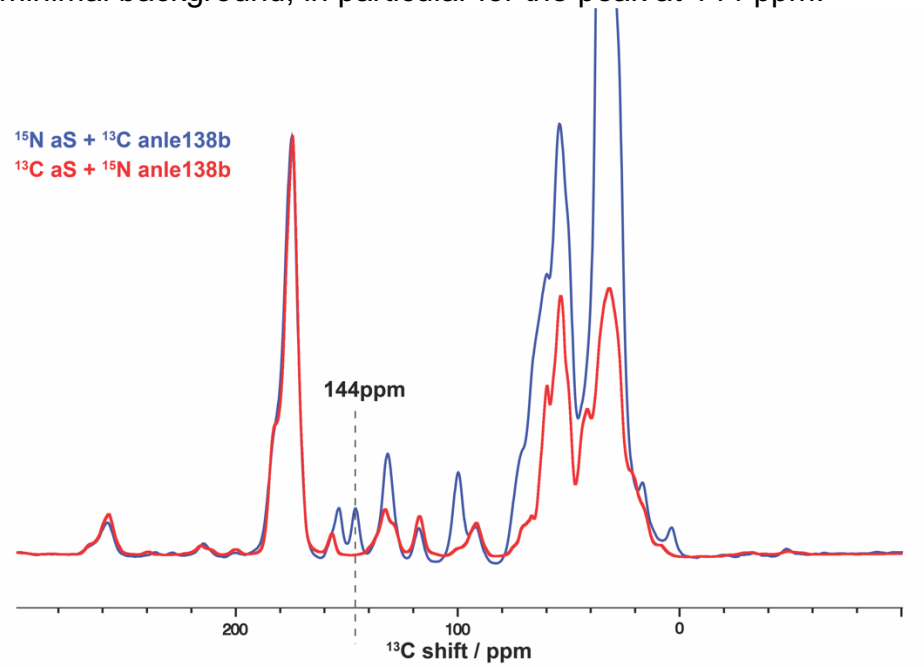

Figure S11 ^{13}C CP-MAS spectra of mixed labelled samples. ^{15}N labelled αS fibril with ^{13}C labelled anle138b is shown in blue and is a sample used for REDOR experiments. ^{13}C-labelled αS fibril with ^{15}N labelled anle138b is in red and is the sample as used for the (H)NHHC experiments. The 144-ppm signal of anle138b (used for the REDOR analyses) is clearly free from any overlapping signals (including sidebands, see the vanishing intensity of the sideband at -50 ppm) arising from the αS fibril.

Estimation of the anle138b:protein ratio in the final sample

Lipids, protein, and anle138b are collected via centrifugation before being backed into the NMR rotor. There is therefore the possibility for differential loss of anle138b or protein. Figure S12 uses the nitrogen signals of anle138b (200 ppm) and protein (120 ppm) to estimate this ratio.

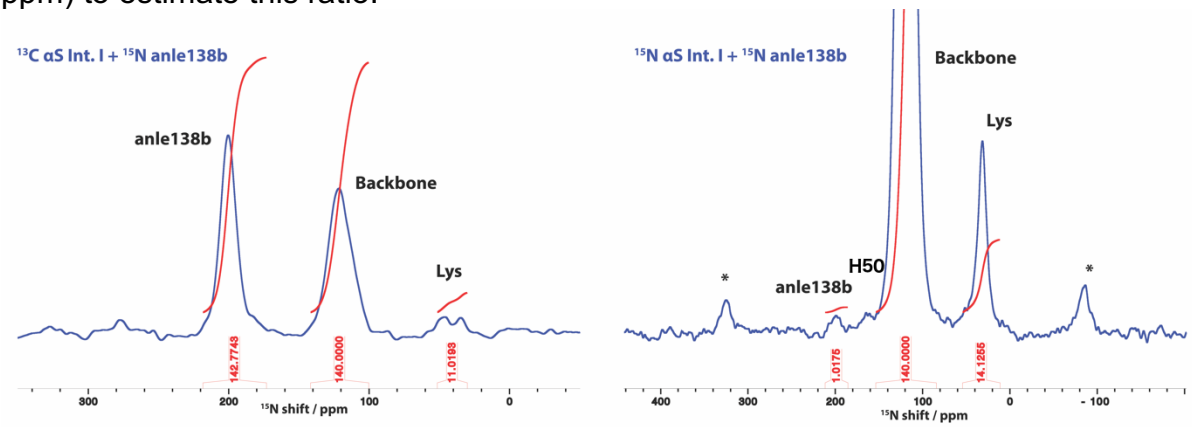

Figure S12 ^{15}N 1D CP-MAS spectra under DNP conditions with microwave ON, of two samples: (left) ^{13}C αS Intermediate-I with ^{15}N anle138b, and (right) ^{15}N αS Intermediate-I with ^{15}N anle138b. Reliable peak integration for anle138b, can only be done for the spectrum on the left. The integrals reveal a 1:1 anle138b/αS amide signal ratio, which closely matches the

expected signal integral ratio of 1:1.1 based on the initial stoichiometry of 1:2 anle138b/protein, 149 amides in the protein (including side chains of N and Q) and natural abundance of ^{15}N of the protein of 0.368 percent. The apparent loss of about 9 percent of the protein is unsurprising, considering that some protein monomer may be left in solution, while essentially all of the very hydrophobic anle138b is expected to remain in the solid lipid/protein pellet. (*) denotes spinning side bands.

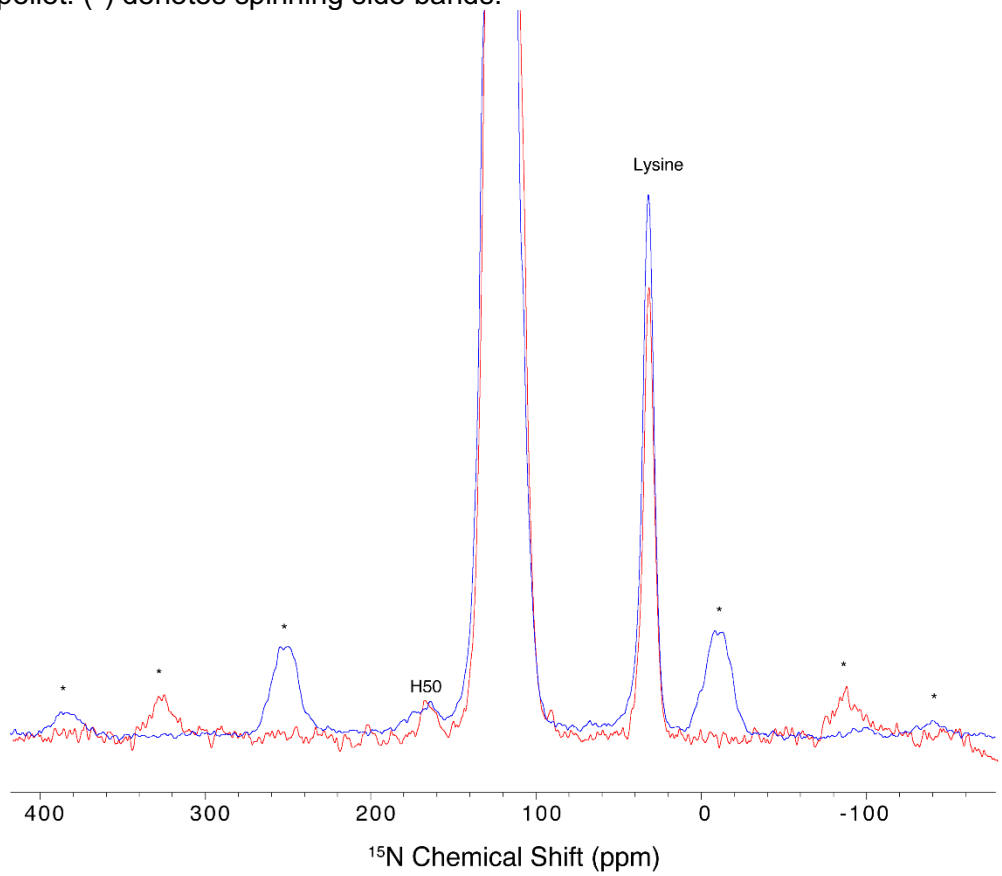

Figure S13 ^{15}N 1D CP-MAS spectra under DNP conditions with microwave ON, of two samples: (blue) ^{13}C αS Intermediate-I with ^{13}C anle138b, and (red) ^{15}N αS Fibrils with ^{13}N anle138b. The H50 resonance at about 165-170 ppm is well separated from the anl138b nitrogen signal in Figure S12. (*) denotes spinning sidebands.

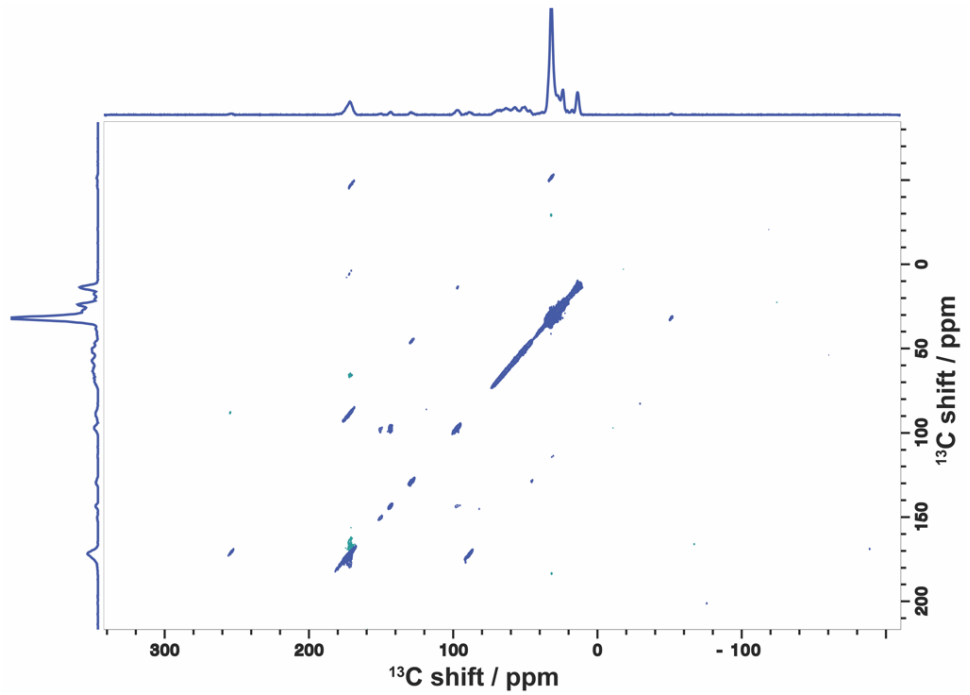

Figure S14 The full ^{13}C-^{13}C 2D correlation spectrum of the ^{15}N labelled αS fibril with ^{13}C labelled anle138b, as shown in Figure 3. The RFDR mixing time was 2.5 ms, the MAS 12.5 kHz, and the sample temperature 100 K (DNP conditions). The spectrum has improved intensity as compared with Fig. 3A by using a different sample. The Fig. 3A data compared the same sample at room temperature and then under DNP conditions.

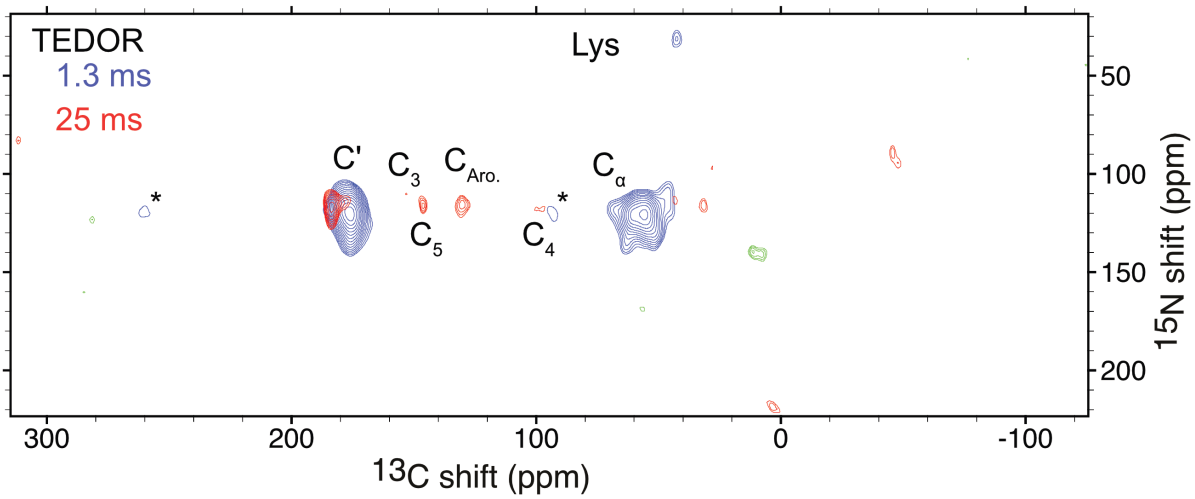

Figure S15 The full ^{13}C-^{15}N 2D z-filtered TEDOR spectra with 1.3 ms (blue) and 25 ms (red) mixing, as shown in Figure 3C. The sample was ^{15}N labelled αS with ^{13}C labelled anle138b. The self-correlation of the anle138b cannot be observed at the expected ^{15}N frequency of 195 ppm and ^{13}C frequencies of 144 and 152 ppm due to low concentration and the low ^{15}N natural abundance. (*) denotes spinning sideband intensity in the 1.3 ms TEDOR spectrum. Negative contours are shown in green and come from the 25 ms data.

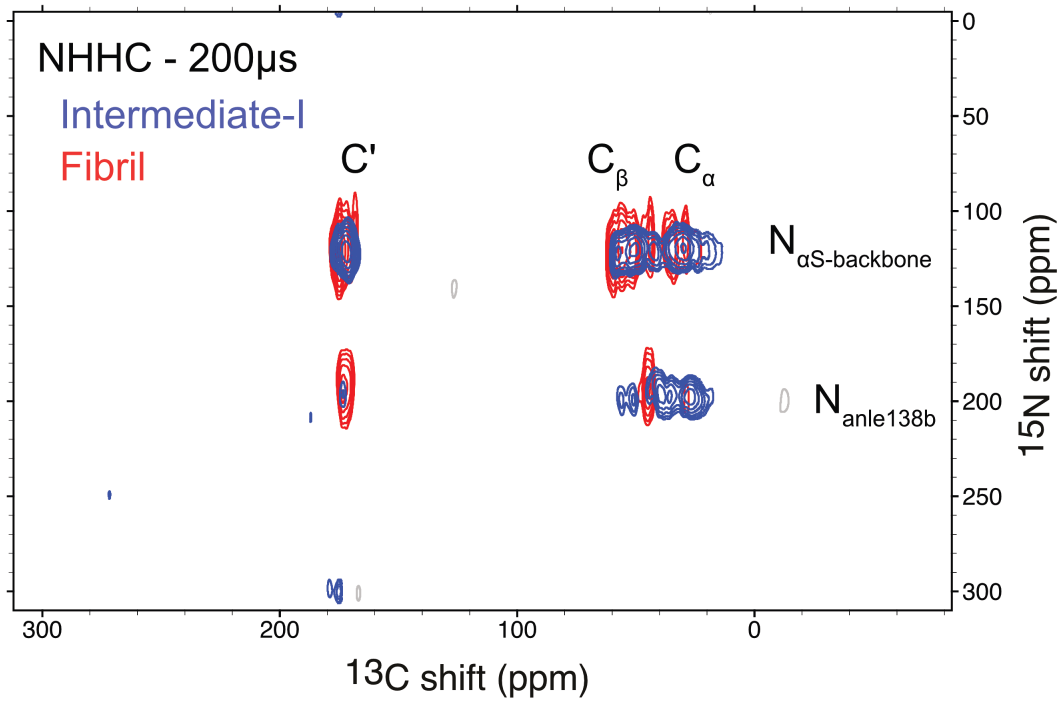

Figure S16 The full ^{15}N-^{13}C 2D NHHC spectral of Figure 4. NHHC mixing was 200 µs, the labeling was ^{13}C αS and ^{15}N anle138b. Fibril is in red and Intermediate-I is in blue.

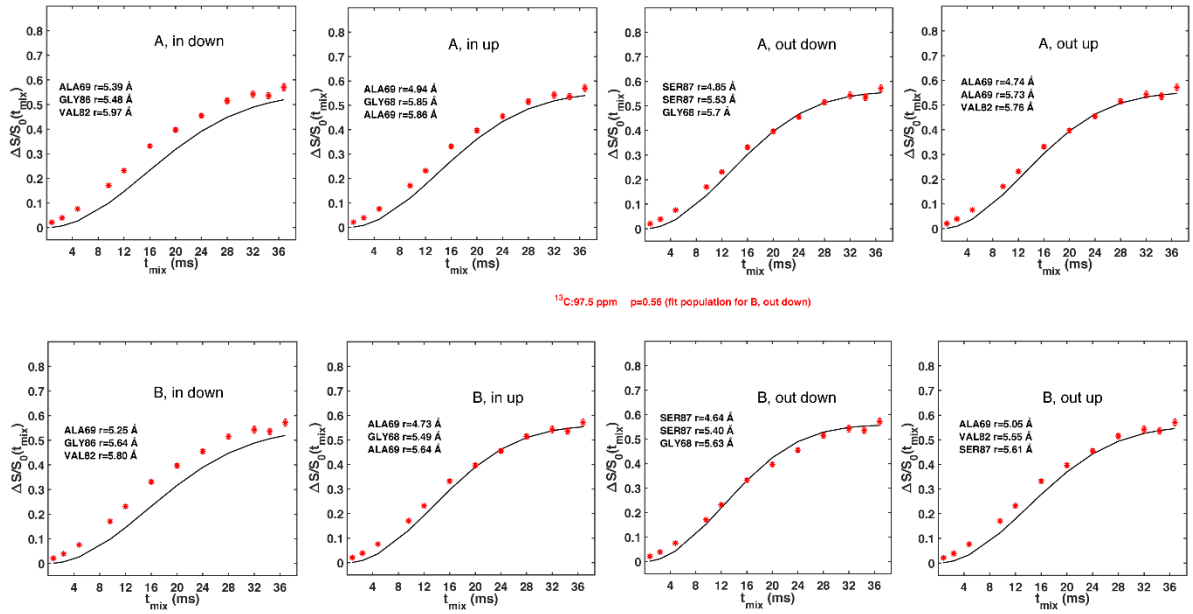

Figure S17 Simulations of REDOR dephasing for additional MD simulation snapshots using the same data as shown in Figure 6. For the snapshots, anle138b is found as one of two tautomers (A or B) and facing in or out and oriented up or down (nomenclature consistent with ref.[13]). The simulation curves are similar in each case. Note that the population of fibril-bound anle138b was kept constant at 0.56, as in Figure 6. The remaining population of anle138b is assumed not to dephase.

Sample preparation for MAS DNP experiments

Fibril or oligomer preparation followed the previously reported procedure.[13-14] Briefly, αS was added to liposomes containing anle138b (1:1 POPC-POPA lipids) at a molar

ratio of 10:1 lipid to protein and allowed to convert into oligomers or fibrils in the presence of pulsed sonication. Approximately ~30 µL volume was obtained after ultracentrifugation, and packed in a standard 3.2 mm zirconia rotor (36 µL total rotor volume accounting for the silicone rubber plug used to seal the DNP rotor). For the comparison sample of Figure S1, data was first measured at room temperature on the 850 MHz magnet, then 5 µL of a 30 mM stock solution of TEMTriPol-1 in DNP juice (^{13}C depleted, d_8 Glycerol/D_2O 60:40) was added in order to reach a 4 mM biradical concentration in the rotor. The glycerol concentration in this case was estimated to be about 30 percent, accounting for some loss of sample during handling. For samples 9 and 10, a concentration of about 60% glycerol was reached by assuming 50-60 percent water remained in the pellet and adding glycerol accordingly. In a later preparation (sample 11 in Table S2), cryoprotectant concentration was better controlled by adding 6 mg of glycerol to the membranous pellet and then removing excess water via vapor diffusion against a 60 percent (by volume) solution of glycerol. The sample had the same enhancement factor of about 40 for protein signals, but reduced intensity from the glycerol. For 60% glycerol samples, polarizing agent was added as lyophilized powder. Due to the sub milligram quantities needed, measurement error was reduced by lyophilizing an aliquot of polarizing agent from an acetonitrile stock solution of the polarizing agent.

Table S2: Summary of samples

Fig. #	Sample #	Date	Fib. or Int.-I	Protein lab.	anle138b lab.	Lipid/Protein ratio	Radical (AmuPol or TEMTriPol-1	Concentration of radical	Glycerol %	Rotor type (Sapphire/Zirconia)	MAS (kHz)	Magnet
2B	1	26.04.2017	F	^{15}N	^{13}C	10	A	10mM	45%	sapphire	8	600
2A,S1	2	06.02.2018	F	^{15}N	^{13}C	10	T	12mM	46%	sapphire	12.5	600
S1	3	23.05.2019	F	^{15}N	^{13}C	10	–	0	0	zirconia	17.5	850
–	4	15.08.2019	F	^{15}N	^{13}C	10	T	7mM	~40%	zirconia	12.5	600
3A	3	23.05.2019	F	^{15}N	^{13}C	10	_	0	0	zirconia	17.5	850
3A	4	15.08.2019	F	^{15}N	^{13}C	10	T	7mM	~40%	zirconia	12.5	600
3C	5	15.05.2018	I	^{15}N	^{13}C	10	T	5mM	~30%	zirconia	12.5	600
S12	6	27.09.2019	F	^{13}C	^{15}N	10	T	5mM	~30%	zirconia	12.5	600
4C,S12	7	27.09.2019	I	^{13}C	^{15}N	10	T	5mM	~30%	zirconia	12.5	600
4C	8	29.10.2018	F	^{13}C	^{15}N	10	T	5mM	~30%	zirconia	12.5	600
2C	9	28.01.2020	F	^{15}N	^{13}C	10	T	5mM	60%	zirconia	12.5	600
2C	10	28.01.2020	F	^{15}N	^{13}C	10	A	5mM	60%	zirconia	12.5	600
6	11	14.03.2022	F	^{15}N	^{13}C	10	A	5mM	60%	zirconia	12.5	600
2D	12	20.06.2022	F	^{13}C	^{15}N*	10	T	8mM	~50%*	zirconia	12.5	600

*This sample contained a related pyrazole (see text) rather than anle138b, and 2 percent DMSO.
–Results similar to those shown in Figure 2A. Data not shown.

Table S3: Amino acid sequence of αS monomer and amino acid composition: MDVFMKGLSKAKEGVVAAAEKTKQGVAEAAGKTKEGVLYVGSKTKEGVVHGVAT VAEKTKEQVTNVGGAVVTGVTAVAQKTVEGAGSIAAATGFVKKDQLGKNEEGAPQ EGILEDMPVDPDNEAYEMPSEEGYQDYEPEA.

Amino acid composition:

Ala (A)	19	13.6%
Arg (R)	0	0.0%
Asn (N)	3	2.1%
Asp (D)	6	4.3%
Cys (C)	0	0.0%
Gln (Q)	6	4.3%
Glu (E)	18	12.9%
Gly (G)	18	12.9%
His (H)	1	0.7%
Ile (I)	2	1.4%
Leu (L)	4	2.9%
Lys (K)	15	10.7%
Met (M)	4	2.9%
Phe (F)	2	1.4%
Pro (P)	5	3.6%
Ser (S)	4	2.9%
Thr (T)	10	7.1%
Trp (W)	0	0.0%
Tyr (Y)	4	2.9%
Val (V)	19	13.6%
Pyl (O)	0	0.0%
Sec (U)	0	0.0%

References:

1. Cavanagh, J.; Skelton, N.; Fairbrother, W.; Rance, M.; Arthur Palmer, I., *Protein NMR Spectroscopy: Principles and Practice*. 2 ed.; Academic Press: 2007.
2. Liu, Y.; Villamena, F. A.; Rockenbauer, A.; Song, Y.; Zweier, J. L., Structural Factors Controlling the Spin–Spin Exchange Coupling: EPR Spectroscopic Studies of Highly Asymmetric Trityl–Nitroxide Biradicals. *Journal of the American Chemical Society* **2013,** *135* (6), 2350-2356.
3. Mathies, G.; Caporini, M. A.; Michaelis, V. K.; Liu, Y.; Hu, K.-N.; Mance, D.; Zweier, J. L.; Rosay, M.; Baldus, M.; Griffin, R. G., Efficient Dynamic Nuclear Polarization at 800 MHz/527 GHz with Trityl-Nitroxide Biradicals. *Angewandte Chemie International Edition* **2015,** *54* (40), 11770-11774.
4. Jähnert, T.; Hager, M. D.; Schubert, U. S., Application of phenolic radicals for antioxidants, as active materials in batteries, magnetic materials and ligands for metal-complexes. *Journal of Materials Chemistry A* **2014,** *2* (37), 15234-15251.
5. Lampp, L.; Azarkh, M.; Drescher, M.; Imming, P., Galvinoxyl radicals: Synthesis of new derivatives, determination of low oxygen contents, and stability studies. *Tetrahedron* **2019,** *75* (18), 2737-2747.
6. Nimerovsky, E.; Goldbourt, A., Insights into the spin dynamics of a large anisotropy spin subjected to long-pulse irradiation under a modified REDOR experiment. *Journal of Magnetic Resonance* **2012,** *225*, 130-141.
7. Zhang, X. C.; Forster, M. C.; Nimerovsky, E.; Movellan, K. T.; Andreas, L. B., Transferred-Rotational-Echo Double Resonance. *The Journal of Physical Chemistry A* **2021,** *125* (3), 754-769.

8. Jaroniec, C. P.; Tounge, B. A.; Rienstra, C. M.; Herzfeld, J.; Griffin, R. G., Measurement of 13C−15N Distances in Uniformly 13C Labeled Biomolecules: J-Decoupled REDOR. *Journal of the American Chemical Society* **1999,** *121* (43), 10237-10238.
9. Gullion, T.; Schaefer, J., Rotational-echo double-resonance NMR. *Journal of Magnetic Resonance (1969)* **1989,** *81* (1), 196-200.
10. Gullion, T., Rotational-Echo, Double-Resonance NMR. In *Modern Magnetic Resonance*, Webb, G. A., Ed. Springer Science & Business Media: Berlin, 2006; pp 713-718.
11. Goetz, J. M.; Schaefer, J., REDOR Dephasing by Multiple Spins in the Presence of Molecular Motion. *Journal of Magnetic Resonance* **1997,** *127* (2), 147-154.
12. Matthes, D.; Gapsys, V.; Griesinger, C.; de Groot, B. L., Resolving the Atomistic Modes of Anle138b Inhibitory Action on Peptide Oligomer Formation. *ACS Chemical Neuroscience* **2017,** *8* (12), 2791-2808.
13. Antonschmidt, L.; Matthes, D.; Dervisoglu, R.; Frieg, B.; Dienemann, C.; Leonov, A.; Nimerovsky, E.; Sant, V.; Ryazanov, S.; Giese, A.; Schroder, G. F.; Becker, S.; de Groot, B. L.; Griesinger, C.; Andreas, L. B., The clinical drug candidate anle138b binds in a cavity of lipidic alpha-synuclein fibrils. *Nat Commun* **2022,** *13* (1), 5385.
14. Antonschmidt, L.; Dervisoglu, R.; Sant, V.; Tekwani Movellan, K.; Mey, I.; Riedel, D.; Steinem, C.; Becker, S.; Andreas, L. B.; Griesinger, C., Insights into the molecular mechanism of amyloid filament formation: Segmental folding of alpha-synuclein on lipid membranes. *Sci Adv* **2021,** *7* (20).